A Novel Solution Process for the Synthesis of VO_2 Thin Films with Excellent Thermochromic Properties

Litao Kang,[†,‡] Yanfeng Gao,*[,†] and Hongjie Luo[†]

Research Center for Industrial Ceramics, Shanghai Institute of Ceramics, Chinese Academy of Sciences, Dingxi 1295, Changning, Shanghai 200050, China, and Graduate University of Chinese Academy of Sciences, Yuquanlu 19, Beijing 100049, China

ABSTRACT This article describes a novel and simple route to preparing VO_2 thermochromic films by using a $VOCl_2$ solution with poly(vinylpyrrolidone) (PVP). X-ray diffraction and Raman spectra showed that the VO_2 films deposited with PVP consisted of a nearly pure monoclinic/rutile (M/R) phase. Conversely, films prepared without PVP contained obviously impure crystalline phases. The as-prepared films with PVP showed excellent optical properties compared to those prepared by common gas-phase methods: an integral visible transmittance of 54.5% and an IR reduction (change in transmittance) of 41.5% at 2000 nm. The phase-transition temperatures were adjusted from 69 to 54 °C by tungsten doping. Equipment analyses revealed that PVP plays two roles in the film formation. First, it fundamentally acts as a film-forming promoter to improve physical gelation via interactions among oppositely charged carbonyl groups and amine groups of the polymer. Second, the negatively charged carbonyl groups can interact with VO^{2+} to form a uniform mixed-gel film after solvent evaporation. Thus, the addition of PVP can stabilize the solution and improve the as-prepared film quality and phase purity. The current study suggests that the process has promise in applications of smart windows.

KEYWORDS: vanadium dioxide • smart window • thermochromic property • polymer • thin film • crystalline phase

1. INTRODUCTION

Among a large number of transition-metal oxides with metal−semiconductor phase transformation characteristics, monoclinic/rutile (M/R)-phase vanadium dioxide (VO_2) is emerging as one of the most important functional materials because of its distinctive optical and electrical properties, which arise from a first-order, fully reversible metal−semiconductor phase transition at approximately 68 °C (1). Moreover, the phase-transition temperature can be further reduced to room temperature by doping, suggesting potential applications as resistive switching elements, thermal relays, optical storage devices, holographic recording media, variable reflectivity mirrors, light modulators, smart windows, and flat panel displays, among others (2).

However, as can be seen in the V−O phase diagram, there are nearly 15−20 stable vanadium oxide phases other than VO_2, such as VO, V_6O_{13}, and V_7O_{13} (3). The formation of VO_2 occurs only at a very narrow oxygen partial pressure of 2 (±0.2)% (3, 4). Furthermore, among more than 10 polymorphs of vanadium dioxide, only the M/R phase undergoes a fully reversible metal−semiconductor phase transition (5). Techniques such as sputtering deposition (6, 7), pulsed laser deposition (PLD) (8, 9), ion implantation (10, 11) and chemical vapor deposition (CVD) (12, 13) have been employed to fabricate M/R-phase VO_2 films, taking advantage of the ability to precisely control the oxygen partial pressure (for example, 0.1244−0.1273 Pa (6), 0.08 Pa (9), 0.0665 and 0.09975 Pa (14)). However, the equipment required for these gas-phase deposition processes is complex and expensive. Alternatively, chemical solution deposition processes can resolve the above problems. Previous studies have focused on the development of a sol−gel method for the deposition of VO_2 films because it has many advantages such as low cost and the option of metal doping (15−18). However, sol−gel methods for the deposition of VO_2 films usually require specific raw materials or treatments (15, 19), which greatly limit their practical application. Therefore, a simple and effective liquid-phase-based method for the deposition of M/R-phase VO_2 films is urgently needed.

In this paper, we report for the first time the development of a novel solution method for the preparation of M/R-phase VO_2 thin films with cheap inorganic vanadium(IV) precursors. This method enables us to prepare VO_2 thin films by spinning precursor solutions and subsequently annealing the gel films. The film-forming mechanism and the effects of PVP on the phase formation have also been studied.

2. EXPERIMENTAL SECTION

2.1. Starting Materials. Vanadium pentoxide (V_2O_5, analytically pure) and diamide hydrochloride ($N_2H_4 \cdot HCl$, analytically pure) were employed as starting materials to prepare a $VOCl_2$ solution. Poly(vinylpyrrolidone) (PVP; K90, K30, and K17) was added as a film-forming promoter, and poly(ethylene glycol) (PEG6000) was also used for comparison. Sodium tungstate dehydrate ($Na_2WO_4 \cdot 2H_2O$, analytically pure) was utilized for

* To whom correspondence should be addressed. E-mail: yfgao@mail.sic.ac.cn. Tel/Fax: +86-21-5241-5270.
Received for review June 1, 2009 and accepted September 3, 2009
† Chinese Academy of Sciences.
‡ Graduate University of Chinese Academy of Sciences.
DOI: 10.1021/am900375k

tungsten doping. All of these regents were bought from Sinopharm Chemical Reagent Co., Ltd., and used without further purification.

2.2. Preparation of the Precursor Solution. A concentrated HCl (38%, 6 mL) solution and a solution containing 1 g of $N_2H_4 \cdot HCl$ were added to an aqueous suspension (50 mL) containing 3.5 g of V_2O_5. After being warmed with stirring, a blue solution formed. The solution was treated with a small amount of V_2O_5 or $N_2H_4 \cdot HCl$ until it contained no VO_2^+ and V^{3+} and was then filtered, and a clear $VOCl_2$ solution (pH $\approx$ 1) was obtained. The detailed manufacturing procedure for the $VOCl_2$ solution can be found in the literature (20). The tungsten-doped VO_2 films could be synthesized by the addition of the proper amount of a 1 mol $\cdot$ L^{-1} $Na_2WO_4 \cdot 2H_2O$ aqueous solution to the $VOCl_2$ solution. The process of sodium ion removal has been described previously (21). Briefly, a concentrated $NH_4 \cdot OH$ (28−30%) aqueous solution was added to the solution to adjust the pH to 6−7. The resulting slurrylike suspension was precipitated by centrifugation and washed several times with deionized water. Next, the precipitate was dispersed in water, and the pH was adjusted to ~1.0 by the addition of an appropriate amount of hydrochloric acid (3.8%). The concentration of the $VOCl_2$ solution was adjusted to 0.1 mol $\cdot$ L^{-1}, and PVP (K30; average molecular weight = 58 000) was added to the solution in gravimetrically determined proportions (6 wt %). This was used as the precursor solution for VO_2 coating. In some experiments, K17 PVP (average molecular weight = 8000), K90 PVP (average molecular weight = 1 300 000), and PEG (average molecular weight = 6000) were also used for comparison.

2.3. Preparation of Films. Films were coated on the fused-silica substrates by spin coating at 400 rpm for 6 s and then 3000 rpm for 30 s. After drying at 60 °C for 10 min to drive off the excess solvent, a smooth thin film of VO_2 precursor was formed. After heat annealing at 600 °C for 3 h in a nitrogen atmosphere, the obtained precursor gel films were transformed into thermochromic VO_2 films (PVP-employing films). For comparison, a VO_2 precursor solution without PVP was also prepared and used to deposit films (PVP-free films). The manufacturing procedure of VO_2 films is under a patenting process, and more details can be found in the examples of patent application document (22).

Caution! *Vanadium precursors are highly toxic. Contact may irritate skin, eyes, and mucous membranes. They may be toxic by ingestion, inhalation, and skin absorption. The effects of contact or inhalation may be delayed.*

2.4. Characterization. Morphologies of the gel powders and films were determined by a JSM-6700F field-emission scanning electron microscope and a JEM-2010 transmission electron microscope. X-ray diffraction (XRD) was carried out on a D/max 2550 V X-ray diffractometer using Cu Kα radiation in the reflection mode. Thermochromic switching characteristics were monitored on a Hitachi U-4100 UV−visible−near-IR spectrophotometer equipped with a film heating unit in the wavelength range of 240−2600 nm. The temperature was measured using a thermocouple in contact with the films and was controlled through a temperature-controlling unit. Hysteresis loops were measured by collecting the transmittance of films at a fixed wavelength (2000 nm) at an approximate interval of 2.0 °C. Raman spectroscopy was performed on a Renishaw invia Raman microscope spectrometer using a 514.5 nm laser at laser output powers of 1 and 20 mW, respectively. The wavelength of the instrument was calibrated before each measurement. Fourier transform infrared (FTIR) spectroscopy was measured with an IRPrestige-21 IR spectrometer at a resolution of 4 cm^{-1}. X-ray photoelectron spectrometry (XPS) was performed with an Axis Ultra DLD instrument using monochromatic Al Kα radiation after 4 keV argon-ion etching for 30 s. XPS data were calibrated to the C 1s peak and analyzed using *XPSPEAK* software version 4.1. Thermogravimetry−differential thermal analysis (TG−DTA) was studied by NETZSCH STA 449C at a heating rate of 10 °C $\cdot$ min^{-1} in a nitrogen atmosphere.

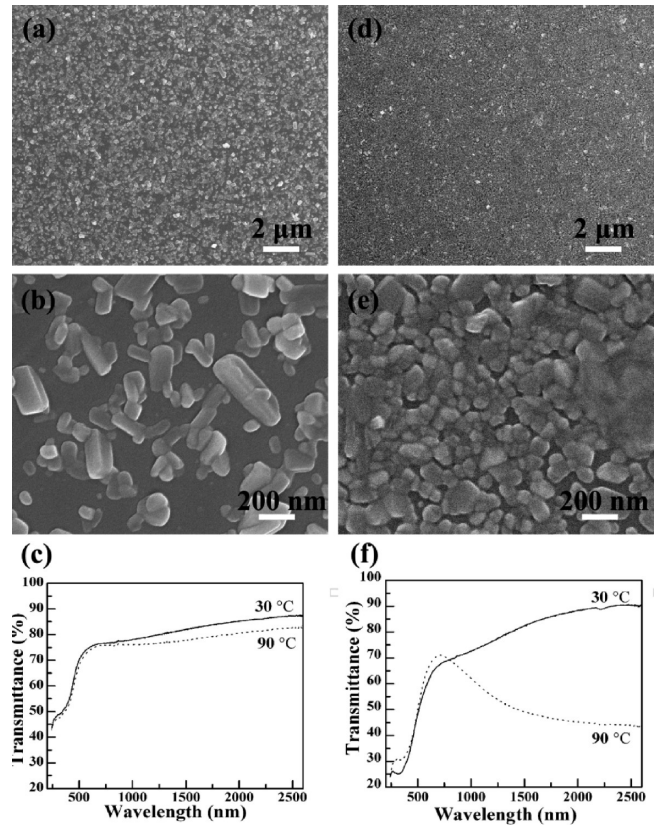

FIGURE 1. SEM images and optical transmittance spectra of a PVP-free film (a−c) and a PVP-employing film (d−f) on fused-silica substrates.

3. RESULTS AND DISCUSSION

3.1. Optical Properties and Microstructures. The films prepared with PVP (PVP-employing) were observed to be light brownish, which is the characteristic color of M/R-phase VO_2 (23). The films without PVP (PVP-free) were almost colorless, indicating that the films without PVP were extremely thin and/or presented different crystalline phases.

The differences in the microstructures of VO_2 films have been clearly observed by scanning electron microscopy (SEM; Figure 1). Both PVP-free and -employing films are particulate and porous, while the particle size of the PVP-employing films (~100 nm in diameter) is much smaller than the PVP-free ones (over ~100 nm), which shows a broad size distribution. The porosity of PVP-free films was obviously larger than that of the PVP-employing films, typically about 63.5% (Figure 1a,b) versus 17% (Figure 1d,e) when they were analyzed with the *Image-pro plus 5.0* software. The thicknesses of the PVP-employing films were determined to be about 50 nm by SEM observation. A series of experiments revealed that the film thicknesses can be varied from 30 to 150 nm by sagaciously choosing the average molecular weight of PVP and/or changing the processing parameters such as spin-coating times, annealing temperatures, and rates. However, the thicknesses of PVP-free films were difficult to be determined because of the

effects from both the roughness of the surfaces and discreteness of the films.

Parts c and f of Figure 1 show the optical properties of the films. In both cases, a metal−semiconductor phase transition is clearly observed. For the PVP-employing films, the optical properties in the visible range as well as the measured IR scope are noteworthy. However, only a very small change in the IR light (2000 nm) has been observed (<5.3%) in the PVP-free film. The mean transparency of the PVP-free film in the visible range is higher than that with PVP, most likely because of the high porosity. The visible transmittance of the PVP-employing films (66% transmittance at 650 nm wavelength) is much better than those made by common gas-phase methods (for example, ≤45% by atmospheric pressure CVD (12), 45% by PLD (1) and 42% by sputtering deposition (7)). The IR reduction at 2000 nm of this film (41.5%; Figure 1f) is comparable to those prepared from the gas phase (1, 12). With regard to the high visible transmittance of our films, it should be noted that the transmittance of PVP-employing films at the starting wavelength of 300 nm is above 25%, higher than that of the reference materials (7, 12). These findings suggest that the films are thin enough or have specific microstructures that permit visible light to partially pass through.

If the effects of voids in the film are discounted, the transmittance of an assumed dense VO_2 film should be 60% at 650 nm, with an IR reduction of 52% at 2000 nm, which are both higher than the values reported by other methods (1, 7, 12). In practice, a thick film with a relatively high density showed a visible transmittance of 59.2% at 650 nm and an IR reduction of 50.2% at 2000 nm, certifying the validity of this estimation for the films prepared with PVP. Similar calculations for the PVP-free film demonstrated that its IR transmittance reduction should be 18%, which is higher than the experimental result (5.3%), probably because of the appearance of impure crystalline phases in the PVP-free films.

3.2. Phase Determination. Because of the film-thickness limits, XRD measurements of both PVP-free and -employing films failed to give the characteristic peaks of VO_2, even by using a glancing-incident model. However, measurements using thick films (about 150 nm) confirmed the existence of a comparative impure phase in the film without PVP.

The XRD results of thick PVP-free films, which were prepared by dropping a precursor solution on the substrates, showed the characteristic peaks of M-phase VO_2 (JCPDS card no. 72-0514, $P21/c$, $a = 0.5743$ nm, $b = 0.4517$ nm, $c = 0.5375$ nm, and $\beta = 122.61°$) along with two weak diffraction peaks at 9.36° and 12.24°, which have not been determinately identified (Figure 2a). However, only peaks of M-phase VO_2 with a preferential orientation along (011) are observed for the thick film with PVP (Figure 2b). The broad background peaks from 15° to 35° in XRD spectra (Figure 2) are assigned to fused-silica substrates.

Figure 3 shows a typical XPS spectrum of a PVP-free VO_2 film. There are only argon, carbon, vanadium, silicon, and

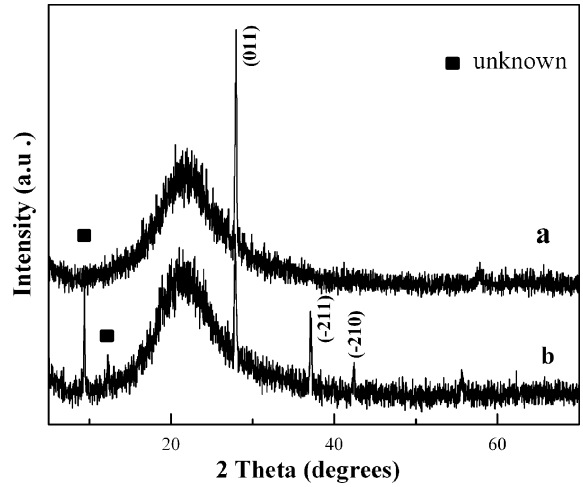

FIGURE 2. XRD patterns of a PVP-employing film (a) and a PVP-free film (b) on fused-silica substrates.

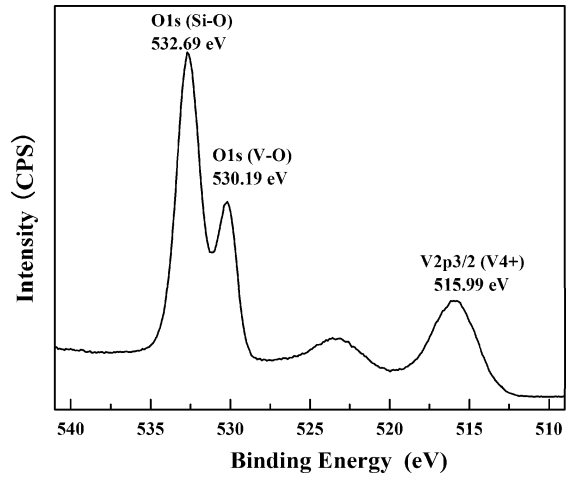

FIGURE 3. High-resolution XPS profiles of V 2p and O 1s of PVP-free films after annealing at 600 °C for 3 h in a nitrogen atmosphere (4 keV argon-ion etching for 30 s).

oxygen in the XPS spectrum after argon-ion etching (40 keV for 30 s), where the carbon and argon peaks are attributed to surface contamination and ion etching, respectively. The binding energy of the V $2p_{3/2}$ peaks centered at 515.99 eV is in good agreement with 515.85 eV of pure VO_2. The difference in the binding energy between O 1s and V $2p_{3/2}$ is 14.2 eV, suggesting that vanadium(IV) was mainly unchanged during annealing (24). From the quantitative analyses of XPS, the PVP-free film has a formula of $VO_{2.127}$, indicating that the film was slightly oxidized.

Therefore, the influence of PVP on crystalline phases should be attributed to the effect of PVP degradation during annealing. Degradation of PVP will definitely release reductive gases that could prevent vanadium(IV) from oxidation. A similar role was also reported for glycerol additions in the preparation of thermochromic VO_2 particles (25). The influence of reductive gases on vanadium(IV) should be weakened when the annealing temperature decreases. When the temperature was lower than 425 °C, the effect of the reductive gas NH_3 almost disappeared (26). However, films with PVP still show obviously higher IR reduction than PVP-free films after annealing at 400 °C, suggesting that the

decomposition of PVP itself may simultaneously favor the formation of M/R-phase VO_2.

3.3. Stability of Precursor Solutions and the Film-Forming Mechanism. In the absence of PVP, the formation of continuous films was difficult, which has been previously ascribed to poor wetting (27). Conversely, the addition of PVP to solutions obviously enhanced the wettability of the solution to the substrate, resulting in the formation of crack-free, uniform films, whereas the explicit relationship between wettability and film formability has not been discussed (27, 28). Therefore, it should be very interesting to further explore the origination of this improvement.

To understand further the above issues, a series of contrast experiments were conducted. Substitution of K90 PVP (average molecular weight = 1 300 000) or K17 PVP (average molecular weight = 8000) for K30 PVP (average molecular weight = 58 000) did not lead to an obvious deterioration of film formability, resulting in only changes of the solution viscosity and film thickness. This result indicated that the average molecular weight of PVP or the steric entangling of the main chains of PVP were not critical reasons for film formability. However, efforts to replace K17 PVP in the precursor solution with PEG (average molecular weight = 6000) failed to give uniform films, even if the wettability of the solution was adjusted with ethanol. Spin coating of a PVP aqueous solution resulted in smooth PVP gel films that covered the whole substrate. Nevertheless, a PEG aqueous solution failed to form gel films, leaving only small isolated droplets. In addition, all of the polymers [poly(vinylpyrrolidone), poly(vinylacetamide), and poly(acrylamide), abbreviated as PVP, PVAcAM, and PAAm, respectively] that were employed to prepare metal oxide films in this process have similar amide groups (27, 28). These polymers were found to be able to improve the film quality (27, 28). Considering the difference between PEG and the previously mentioned polymers with amide groups (PVP, PVAcAM, and PAAm), we believe that interactions among amide groups of these polymers enhance the film qualities, aside from their improvement of wettability.

In PVP molecules, nitrogen atoms of the amide groups partially donate their lone-pair electrons to neighboring carbon atoms in the carbonyl groups through orbit conjugation (29), resulting in negatively charged carbonyl groups and positively charged amine groups (29, 30). It has been reported that electrostatic interactions between carboxylate and ammonium and between ammonium and sulfonic acid could be employed to maintain the overall integrity of gel films containing two polymers (31). Accordingly, it is reasonable to speculate that some of the negatively charged carbonyl groups will interact with the positively charged amine groups of other molecules, forming a cross-linked polymer gel film. Additionally, the steric entangling of the polymer chains possibly assists in the enhancement of cross-linking.

It was also found that precursor solutions without PVP were unstable, with a large amount of precipitates being formed after aging for several days. However, PVP-employing solutions remained stable for several months, with only a few precipitates suspending in the solution, indicating that PVP improved the stability of the precursor solution probably because the negatively charged carbonyl groups bind VO^{2+} to form a relatively stable precursor solution. To examine the interactions between PVP and VO^{2+}, FTIR spectroscopy was employed to characterize the precursor solution with or without PVP at the same pH value (0.96). The results are shown in Figure 4. For comparison, FTIR spectra of PVP (Figure 4a) and PVP at the pH value employed (adjusted with H_2SO_4; Figure 4b) are also included.

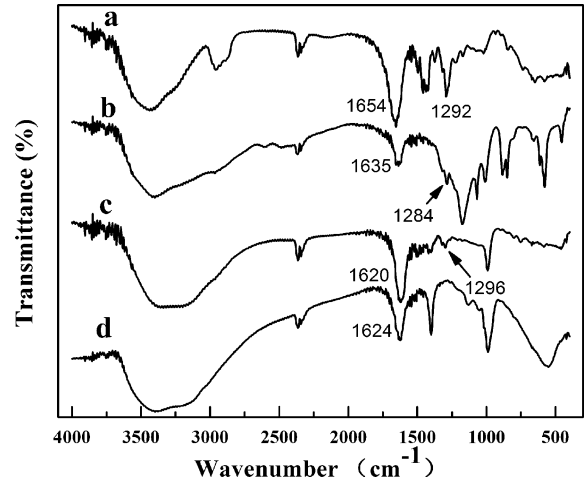

FIGURE 4. FTIR spectra of PVP (a), PVP with H_2SO_4 (b), a precursor solution with PVP (c), and a $VOCl_2$ precursor solution (d). The pH values of parts b–d were adjusted to be the same (0.96).

Generally, the strong and sharp peak at 1654 cm^{-1} is assigned to the stretching vibration of −C═O, and the peak at 1292 cm^{-1} is attributed to −C−N vibrations (Figure 4a) (32). When H_2SO_4 was added to PVP (Figure 4b), the stretching vibration of −C═O shifted to a lower wavenumber of 1635 cm^{-1}, which originates from the loosening of the −C═O double bond by coordination between negatively charged carbonyl groups and H^+ (33). In precursor solutions with PVP (Figure 4c), the frequency of the −C═O stretching vibration was lower (1620 cm^{-1}) because of the influence of VO^{2+}. The coordination interactions between the carboxyl groups of PVP and metal ions (lithium, calcium, cobalt, and silver) have also been reported in PVP−*N*,*N*-dimethylformamide (DMF)−MCl_n systems (34) and polymer/silver salt complex membranes (35–37). Although the vibration at 1624 cm^{-1} in the spectrum for a PVP-free precursor solution was poorly identified (Figure 4d), the −C−N vibration remained almost unchanged (Figure 4a–c) for all of these gel precursors, indicating that there were no interactions between the amine groups and VO^{2+}. According to the above discussion, the effects of PVP on the stabilization of the precursor solution were due to interactions of the negatively charged carbonyl groups in PVP with VO^{2+}. Furthermore, it has been reported that the interactions between the metal ions and the carbonyl groups from different PVP molecules increase the apparent viscosity of the PVP−DMF−MCl_n solution (M = Li, Ca, or Co) (34), where metal ions act as cross-linking points between different PVP molecular chains (34), improving the film formability. This improvement was

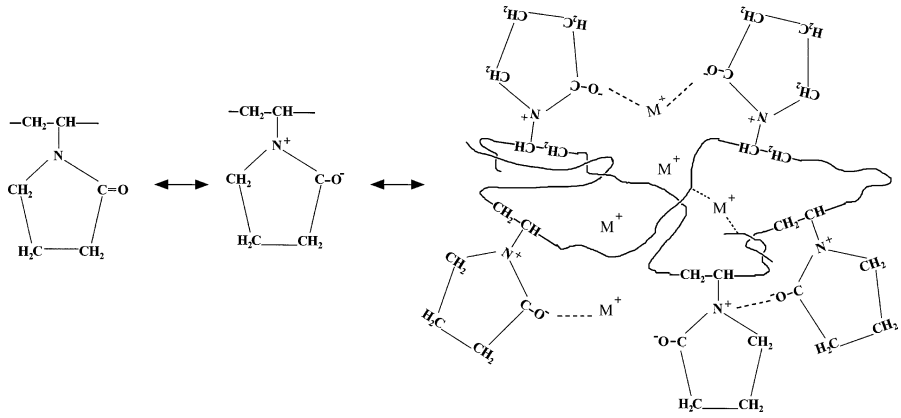

FIGURE 5. Schematic illustration of the interactions between VO^{2+} (M^{+}) and PVP as well as the film-forming mechanism.

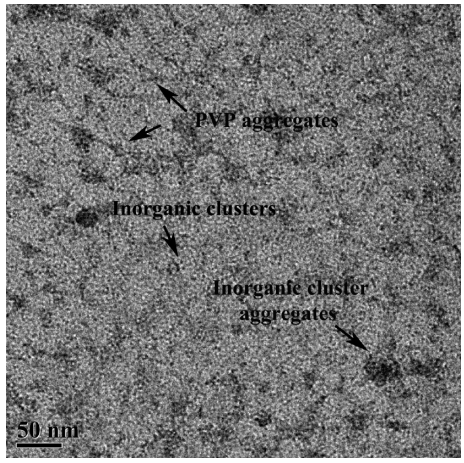

FIGURE 6. TEM image of a precursor gel.

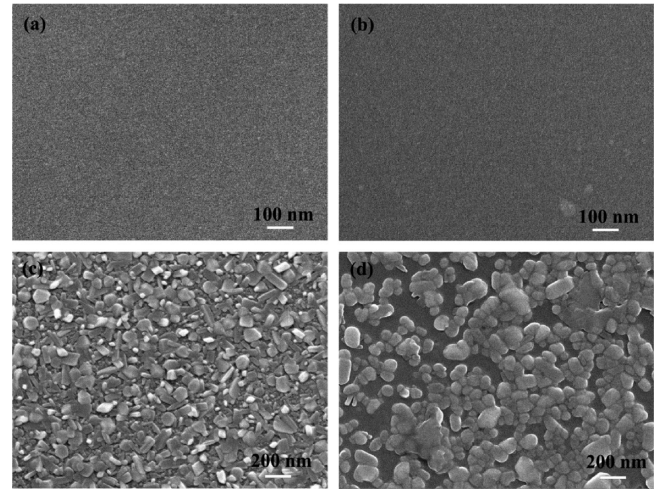

FIGURE 7. SEM images of precursor gel films that underwent annealing under a nitrogen atmosphere for 3 h at 60 (a), 200 (b), 400 (c), and 600 °C (d).

observed in both PVP- and PEG-employing precursor solutions, although the latter was still inadequate to fabricate uniform films.

A schematic illustration of the film-forming mechanism is given in Figure 5. The interactions among polymer molecules via the oppositely charged groups, along with those between the carbonyl groups and the metal ions, ensure the formation of cross-linked high-quality gel films after solvent evaporation. In addition, steric entangling of the polymer chains enhances the cross-linking.

3.4. Morphologies of Precursor Gels and Morphology Evolution of Gel Films. To verify the above discussion, a systematic electron microscopy investigation was conducted. Transmission electron microscopy (TEM) images of the PVP-employing precursor gels were taken after solvent evaporation, and the results are shown in Figure 6. Different from the conventional sol solution that was defined as a stable suspension of colloidal solid particles dispersed in a liquid medium (38), no obvious sol particles (≥5 nm) were found, suggesting that the precursor solution was in a solution state rather than a sol state. In this image, two homogeneous mixed aggregates with different morphologies were observed. Isolated dark spherical clusters were assigned as vanadium-related phases. Filamentous particles were probably from the polymer phases that entangled with each other after solvent evaporation. The existence of PVP macromolecular filamentous particles enhanced the formation of high-quality films.

Morphology evolution of the PVP-employing gel films with different annealing temperatures for 3 h was also observed, and the results are shown in Figure 7. After heating at 60 and 200 °C (Figure 7a,b), smooth and uniform films without any observable microcracks or granular precipitates were obtained, suggesting the formation of a uniform mixed-gel film. Moreover, these films were soluble in water and could easily be washed away, indicating that the bonds that were responsible for the reversible gelation were weak enough to be destroyed by dilution. These bonds were introduced completely by the polymers, should be altered by polymer choice, and should be diverse enough for the preparation of different metal oxide films. The polymer-assisted gelation process of the precursor solution that allows the deposition of high-quality films from inorganic salts might be the most obvious and important advantage of this method over the conventional sol–gel process.

After heating at 400 °C (Figure 7c), decomposition of PVP occurred and grains appeared. These films became blue, which is the characteristic color of metastable B-phase VO_2. B-phase VO_2 always exists at low temperatures (≤450 °C) (20, 39). Optical analyses revealed that these films showed weak thermochromic properties, indicating that there were

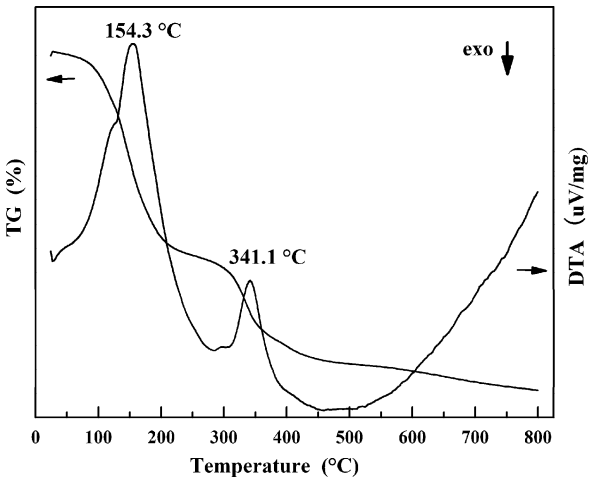

FIGURE 8. TG–DTA curves of the precursor gel in a nitrogen atmosphere.

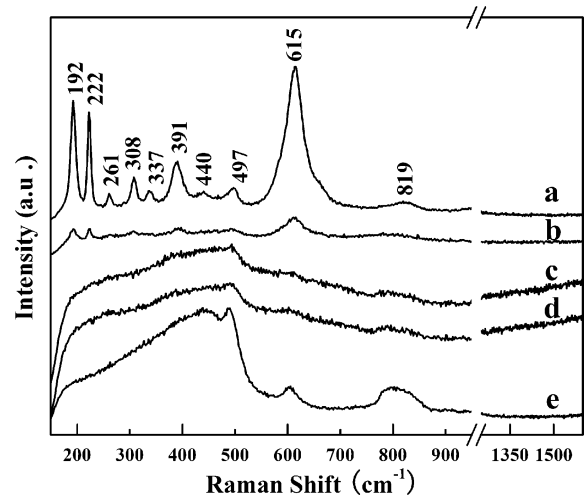

FIGURE 9. Output power dependence of Raman spectra for PVP-employing VO_2 films on fused-silica substrates and a substrate only: (a) 1 mW for a VO_2 film, (b) 1 mW for a $V_{0.99}W_{0.01}O_2$ film, and (c–e) 20 mW for a VO_2 film, a $V_{0.99}W_{0.01}O_2$ film, and a substrate, respectively.

only very small quantities of M/R-phase VO_2 crystallites in these films. Subsequent Raman and XRD measurements failed to give characteristic peaks of either B- or M/R-phase VO_2, even with a thick film undergoing the same annealing process. Likewise, PVP-free films did not show any evidence of crystallization, and this is currently under study. The grain size distribution became narrow, while large amounts of voids emerged after heating at 600 °C for 3 h (Figure 7d), probably because of shrinkage during heat treatment.

TG–DTA of the gel precursor (26.73 mg) under a flow of nitrogen was also carried out to determine potential reactions during heat treatment (Figure 8). There were two main endothermic peaks centered at 154.3 and 341.1 °C in DTA, with two sudden weight losses at corresponding temperatures in the TG curve, which can be attributed to the evaporation of adsorbed water and the degradation of the polymer, respectively. This TG–DTA result agrees well with the SEM observations and can be used to explain the morphology evolution. The exothermic peak at 387 °C corresponding to the crystallization of VO_2 was not found (20), suggesting that the crystallization temperature of VO_2 overlaps with the degradation temperature of PVP. It has been reported that a short duration at low temperature is favorable for the formation of the desired M/R-phase VO_2 (19). Before the degradation of PVP, the formation of metal oxides does not occur because the metals are fixed by the polymers. The decomposition of the polymer probably induces the formation of a pure R/M phase, as shown in section 3.2 of the experimental results. A similar influence of polymer decomposition on crystallization has also been described in other systems (40–42).

3.5. Tungsten Doping and Phase-Transition Temperatures. To reduce the transition temperatures, tungsten-doped PVP-employing films were fabricated. Figure 9 shows Raman spectra that were performed on pure and tungsten-doped VO_2 films. At an output power of 1 mW (Figure 9a) on a pure film, an almost complete set of Raman bands of M-phase VO_2 was observed. The bands agree well with the reported data for M-phase VO_2, with centers at 192 [192 (23), 195 (43), 191 (44)], 222 [223 (23), 222 (43), 221 (44)], 261 [261 (23), 264 (43), 258 (44)], 308 [310 (23), 304 (43), 308 (44)], 337 [338 (43), 335 (44)], 391 [390 (23), 392 (43, 44)], 440 [439 (43)], 497 [500 (23), 496 (43), 497 (44)], 615 [622 (43), 612 (23, 44)], and 816 [825 (43)] cm^{-1}. There is at least one corresponding band for every Raman band of our film. A Raman spectrum of a $V_{0.99}W_{0.01}O_2$ film (Figure 9b; this formula represents the atomic percent in the feed) at 1 mW showed only weak bands, suggesting that the film was at the phase-transition point because of the reduction effect of the tungsten doping on the transition temperature. No Raman bands appeared at an output power of 20 mW for either of the films (Figure 9c,d), indicating that the complete phase transition from M-phase VO_2 to R-phase VO_2 occurred at this output power (43). The contribution of a fused-quartz substrate has also been included (Figure 9e) for the sake of comparison. Although an overlap of the Raman bands of the fused quartz and WO_3 at 807 cm^{-1} makes it difficult to determine the presence of WO_3 in the enlarged Raman spectra of tungsten-doped films, other strong Raman bands located at 716 and 275 cm^{-1} were not observed (45), excluding the absence of WO_3. The absence of any significant impurity band, such as V_2O_5 phases with Raman shifts at around 700 and 994 cm^{-1} (2) or disordered/graphite carbon with Raman shifts at around 1320 and 1591 cm^{-1} (46, 47), indicates that there were no obvious impure vanadium oxides or residual carbon.

To determine the phase-transition temperatures of the obtained films, hysteresis loops of pure and tungsten-doped VO_2 films were measured by recording transmittances and temperatures of these films at a fixed optical wavelength (2000 nm). As seen in Figure 10, a pure VO_2 film shows a hysteresis loop width of 31 °C at mean transmittance, which is much larger than that of pure VO_2 films on glass (11.1 (16) and 8 °C (7)) but is comparable to that of VO_2–SiO_2 composite films (10, 48). Hysteresis widening can be attributed to the states of grain boundaries (crystallographic misorientations and voids at boundaries, etc.) introduced by the substrate and/or the amorphous precursor, as has been

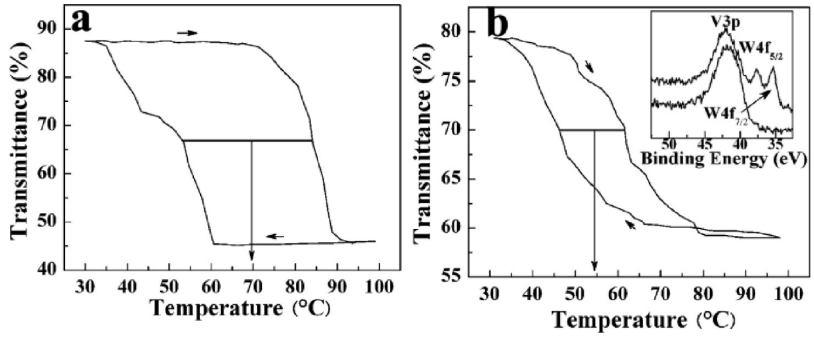

FIGURE 10. Temperature dependence of the optical transmittance at a fixed wavelength (2000 nm) for a VO_2 film (a) and a $V_{0.99}W_{0.01}O_2$ film (b). The inset shows the W $4f_{5/2}$ and W $4f_{7/2}$ spectra for a VO_2 film (bottom) and a $V_{0.99}W_{0.01}O_2$ film (top).

discussed by Narayan and Bhosle (8). The mean phase-transformation temperature is about 69 °C (Figure 10a), which is very close to that of a stoichiometric bulk single crystal of VO_2. This result indicates that these substrates have almost no effect on the phase-transition temperature in this process.

The $V_{0.99}W_{0.01}O_2$ film exhibited a hysteresis loop centered at 54 °C with a width of 16 °C (Figure 10b), implying a decrease in the phase-transition temperature of about 15 °C. This decreasing efficiency is less than described in other reports (12, 13). Significantly, the decreasing efficiency of the phase-transition temperature for the $V_{0.99}W_{0.01}O_2$ film was lower than the average efficiencies of other doping doses in other reports, which employed doping processes similar to those used to prepare VO_2 particles (21), likely because the tungsten ions were not completely incorporated into the final VO_2 films. W $4f_{5/2}$ and W $4f_{7/2}$ XPS peaks with binding energies of 37.7 and 35.3 eV, respectively, are clearly seen in the Figure 10b inset for the tungsten-doped thin films (the tungsten ion in these films is W^{6+} according to the standard binding energy). The width narrowing of the hysteresis loop can be explained by the martensitic transformation model for VO_2 (49). Tungsten doping increases the density of the structural defects, a power function of the driving force, which reduces the activation energy of the coordinated jumps of V^+ cations (phase transitions take place at a certain defect density for fixed-size crystal grains) (8). The activation energy further influences the width of the hysteresis loops via degrees of supercooling or superheating. This deduction of the martensitic transformation model is in agreement with various experimental results (6, 50−52).

4. CONCLUSIONS

In conclusion, we have successfully prepared M/R-phase VO_2 films through the deposition of a precursor solution with PVP. It was found that the polymer additive PVP not only acted as a film-forming promoter but also facilitated the formation of M/R-phase VO_2. The effect of PVP on the crystalline phase was attributed to overlaps of the crystallization temperature of VO_2 with the degradation temperature of PVP and the influence of PVP on the atmosphere, while the film-forming promoting effect was attributed to the formation of a cross-linked gel film through the interactions of oppositely charged functional groups of the polymer molecules with VO^{2+}. Furthermore, the as-prepared films showed excellent optical properties compared to those prepared by common gas-phase methods, with an integral visible transmittance of 54.5% and an IR reduction of 41.5% at 2000 nm. The phase-transition temperatures were adjusted by tungsten doping, with centers at 69 and 54 °C and hysteresis loop widths of 31 and 16 °C for the VO_2 and $V_{0.99}W_{0.01}O_2$ films, respectively.

Acknowledgment. This study was supported, in part, by the Century Program (One-Hundred-Talent Program) of the Chinese Academy of Sciences, National Key Basic Research Program (Grant 2009CB939900), the National Natural Science Foundation of China (Contract 50772126), and Shanghai Key Basic Research Program (Grant 09DJ1400200).

REFERENCES AND NOTES

(1) Maaza, M.; Bouziane, K.; Maritz, J.; McLachlan, D. S.; Swanepool, R.; Frigerio, J. M.; Every, M. *Opt. Mater.* **2000**, *15*, 41–45.
(2) Gurvitch, M.; Luryi, S.; Polyakov, A.; Shabalov, A.; Dudley, M.; Wang, G.; Ge, S.; Yakovlev, V. *J. Appl. Phys.* **2007**, *102*, 033504.
(3) Nag, J.; Haglund, R. F. *J. Phys.: Condes. Matter.* **2008**, *20*, 264016.
(4) Balu, R.; Ashrit, P. V. *Appl. Phys. Lett.* **2008**, *92*, 021904.
(5) Cao, C. X.; Gao, Y. F.; Luo, H. J. *J. Phys. Chem. C* **2008**, *112*, 18810–18814.
(6) Chen, S. H.; Ma, H.; Dai, J.; Yi, X. J. *Appl. Phys. Lett.* **2007**, *90*, 101117.
(7) Lee, M.-H.; Cho, J.-S. *Thin Solid Films* **2000**, *365*, 5–6.
(8) Narayan, J.; Bhosle, V. M. *J. Appl. Phys.* **2006**, *100*, 103524.
(9) Wang, Y. L.; Chen, X. K.; Li, M. C.; Wang, R.; Wu, G.; Yang, J. P.; Han, W. H.; Cao, S. Z.; Zhao, L. C. *Surf. Coat. Technol.* **2007**, *201*, 5344–5347.
(10) Lopez, R.; Boatner, L. A.; Haynes, T. E.; Haglund, R. F.; Feldman, L. C. *Appl. Phys. Lett.* **2001**, *79*, 3161–3163.
(11) Lopez, R.; Boatner, L. A.; Haynes, T. E.; Feldman, L. C.; Haglund, R. F. *J. Appl. Phys.* **2002**, *92*, 4031–4036.
(12) Binions, R.; Hyett, G.; Piccirillo, C.; Parkin, I. P. *J. Mater. Chem.* **2007**, *17*, 4652–4660.
(13) Manning, T. D.; Parkin, I. P. *J. Mater. Chem.* **2004**, *14*, 2554–2559.
(14) Petit, C.; Frigerio, J. M.; Goldmann, M. *J. Phys.: Condes. Matter.* **1999**, *11*, 3259–3264.
(15) Chae, B. G.; Kim, H. T.; Yun, S. J.; Kim, B. J.; Lee, Y. W.; Youn, D. H.; Kang, K. Y. *Electrochem. Solid State Lett.* **2006**, *9*, C12–C14.
(16) Chen, H. K.; Hung, H. C.; Yang, T. C. K.; Wang, S. F. *J. Non-Cryst. Solids* **2004**, *347*, 138–143.
(17) Mai, L. Q.; Hu, B.; Hu, T.; Chen, W.; Gu, E. D. *J. Phys. Chem. B* **2006**, *110*, 19083–19086.
(18) Beteille, F.; Mazerolles, L.; Livage, J. *Mater. Res. Bull.* **1999**, *34*, 2177–2184.
(19) Yuan, N. Y.; Li, J. H.; Lin, C. L. *Appl. Surf. Sci.* **2002**, *191*, 176–180.
(20) Zheng, C. M.; Zhang, J. L.; Luo, G. B.; Ye, J. Q.; Wu, M. M. *J. Mater. Sci.* **2000**, *35*, 3425–3429.
(21) Shi, J. Q.; Zhou, S. X.; You, B.; Wu, L. M. *Sol. Energy Mater. Sol. Cells* **2007**, *91*, 1856–1862.

(22) Gao, Y. F.; Kang, L. T.; Luo, H. J. Vanadium Precursor Solution, VO_2 Thin Films and Methods of Manufacturing Same. China Patent Appl. No. 200810205226.X. Filed on Dec 31 2008.
(23) Manning, T. D.; Parkin, I. P.; Clark, R. J. H.; Sheel, D.; Pemble, M. E.; Vernadou, D. *J. Mater. Chem.* **2002**, *12*, 2936–2939.
(24) Silversmit, G.; Depla, D.; Poelman, H.; Marin, G. B.; De Gryse, R. *J. Electron Spectrosc. Relat. Phenom.* **2004**, *135*, 167–175.
(25) Bai, H. P.; Cortie, M. B.; Maaroof, A. I.; Dowd, A.; Kealley, C.; Smith, G. B. *Nanotechnology* **2009**, *20*, 9.
(26) Zheng, C. M.; Zhang, X. M.; Zhang, J. H.; Liao, K. R. *J. Solid State Chem.* **2001**, *156*, 274–280.
(27) Kozuka, H.; Kishimoto, T. *Chem. Lett.* **2001**, 1150–1151.
(28) Kishimoto, T.; Kozuka, H. *J. Mater. Res.* **2003**, *18*, 466–474.
(29) *Organic Chemistry;* Lu, G. Y., Ed.; Nanjing University Press: Nanjing, China, 1999; p 269.
(30) Pattanaik, M.; Bhaumik, S. K. *Mater. Lett.* **2000**, *44*, 352–360.
(31) Chia, K. K.; Cohen, R. E.; Rubner, M. F. *Chem. Mater.* **2008**, *20*, 6756–6763.
(32) Yuan, X. P.; Li, C. C.; Guan, G. H.; Xiao, Y. N.; Zhang, D. *J. Appl. Polym. Sci.* **2009**, *111*, 566–575.
(33) Wang, Z. D.; Xu, Z. L.; Yang, Y. G.; Li, S. X. *Mater. Rev. (Chongqing, P. R. China) Special Issue VII* **2006**, *20*, 53–57 (in Chinese).
(34) Hao, C. W.; Zhao, Y.; Zhou, Y.; Zhou, L. J.; Xu, Y. Z.; Wang, D. J.; Xu, D. F. *J. Polym. Sci., Part B: Polym. Phys.* **2007**, *45*, 1589–1598.
(35) Kim, J. H.; Kim, C. K.; Won, J.; Kang, Y. S. *J. Membr. Sci.* **2005**, *250*, 207–214.
(36) Kim, J. H.; Min, B. R.; Won, J.; Kang, Y. S. *Chem.—Eur. J.* **2002**, *8*, 650–654.
(37) Hong, S. U.; Jin, J. H.; Won, J.; Kang, Y. S. *Adv. Mater.* **2000**, *12*, 968–971.
(38) Hiemenz, P. C. *Principles of Colloid and Sruface Chemsiry*; Marcel Dekker: New York, 1977.
(39) Liu, X.; Xie, G.; Huang, C.; Xu, Q.; Zhang, Y.; Luo, Y. *Mater. Lett.* **2008**, *62*, 1878–1880.
(40) Luo, H. M.; Jain, M.; McCleskey, T. M.; Bauer, E.; Burrell, A. K.; Jia, Q. X. *Adv. Mater.* **2007**, *19*, 3604–3607.
(41) Jia, Q. X.; McCleskey, T. M.; Burrell, A. K.; Lin, Y.; Collis, G. E.; Wang, H.; Li, A. D. Q.; Foltyn, S. R. *Nat. Mater.* **2004**, *3*, 529–532.
(42) Burrell, A. K.; McCleskey, T. M.; Jia, Q. X. *Chem. Commun.* **2008**, 1271–1277.
(43) Kim, H. T.; Chae, B. G.; Youn, D. H.; Kim, G.; Kang, K. Y.; Lee, S. J.; Kim, K.; Lim, Y. S. *Appl. Phys. Lett.* **2005**, *86*, 242101.
(44) Petrov, G. I.; Yakovlev, V. V.; Squier, J. *Appl. Phys. Lett.* **2002**, *81*, 1023–1025.
(45) Lethy, K. J.; Beena, D.; Kumar, R. V.; Pillai, V. P. M.; Ganesan, V.; Sathe, V.; Phase, D. M. *Appl. Phys. A: Mater. Sci. Process.* **2008**, *91*, 637–649.
(46) Pol, V. G.; Calderon-Moreno, J. A.; Thiyagarajan, P. *Langmuir* **2008**, *24*, 13640–13645.
(47) Pol, V. G.; Pol, S. V.; Perkas, N.; Gedanken, A. *J. Phys. Chem. C* **2007**, *111*, 134–140.
(48) Sidorov, A. I.; Vinogradova, O. P.; Obyknovennaya, I. E.; Khrushchova, T. A. *Tech. Phys. Lett.* **2007**, *33*, 581–582.
(49) Lopez, R.; Haynes, T. E.; Boatner, L. A.; Feldman, L. C.; Haglund, R. F. *Phys. Rev. B* **2002**, *65*, 224113.
(50) Suh, J. Y.; Lopez, R.; Feldman, L. C.; Haglund, R. F. *J. Appl. Phys.* **2004**, *96*, 1209–1213.
(51) Vernardou, D.; Pemble, M. E.; Sheel, D. W. *Chem. Vap. Deposition* **2007**, *13*, 158–162.
(52) Burkhardt, W.; Christmann, T.; Meyer, B. K.; Niessner, W.; Schalch, D.; Scharmann, A. *Thin Solid Films* **1999**, *345*, 229–235.

AM900375K